






# OCA-B/Pou2af1 is sufficient to promote CD4<sup>+</sup> T cell memory and prospectively identifies memory precursors

Wenxiang Sun<sup>a,b,1</sup>, Erik P. Hughes<sup>a,b,1</sup> , Heejoo Kim<sup>a,b,1,2</sup>, Jelena Perovanovic<sup>a,b,3</sup>, Krystal R. Charley<sup>a,b</sup>, Bryant Perkins<sup>a</sup>, Junhong Du<sup>a,b</sup>, Andrea Ibarra<sup>a,b</sup>, Amber R. Syage<sup>a,b</sup>, J. Scott Hale<sup>a</sup>, Matthew A. Williams<sup>a,b</sup> , and Dean Tantin<sup>a,b,4</sup> 

Edited by Rafi Ahmed, Emory University, Atlanta, GA; received May 31, 2023; accepted January 12, 2024

The molecular mechanisms leading to the establishment of immunological memory are inadequately understood, limiting the development of effective vaccines and durable antitumor immune therapies. Here, we show that ectopic OCA-B expression is sufficient to improve antiviral memory recall responses, while having minimal effects on primary effector responses. At peak viral response, short-lived effector T cell populations are expanded but show increased *Gadd45b* and *Socs2* expression, while memory precursor effector cells show increased expression of *Bcl2*, *Il7r*, and *Tcf7* on a per-cell basis. Using an OCA-B mCherry reporter mouse line, we observe high OCA-B expression in CD4<sup>+</sup> central memory T cells. We show that early in viral infection, endogenously elevated OCA-B expression prospectively identifies memory precursor cells with increased survival capability and memory recall potential. Cumulatively, the results demonstrate that OCA-B is both necessary and sufficient to promote CD4<sup>+</sup> T cell memory in vivo and can be used to prospectively identify memory precursor cells.

immunological memory | CD4 T cells | Pou2af1/OCA-B

The ability to respond robustly to secondary antigen exposures (immune memory) is a defining feature of the adaptive immune system and forms the physiologic basis for vaccination (1). Immune memory can also drive autoimmune and antitumor responses (2–5). Strategies that promote memory have the potential to improve both vaccine efficacy and tumor immunotherapy. Central memory T cells (T<sub>CM</sub>), which home to secondary lymphoid organs, are particularly long lived and demonstrate high proliferative capacity upon antigen reencounter.

Multiple transcription factors and epigenetic regulators are known to modulate T<sub>CM</sub> formation or function, including Id3 (6), Blimp1 (7–9), Suv39h1 (10), T-bet (11, 12), Foxo1 (13, 14), Bcl6 (15, 16), Eomes (17), and TCF1 (18). Many of these factors regulate memory more clearly in CD8<sup>+</sup> compared to CD4<sup>+</sup> T cells. In CD4<sup>+</sup> T cells, the lymphocyte-restricted transcriptional coregulator OCA-B (also known as OBF-1 and Pou2af1) is induced upon T cell antigen stimulation (19, 20). T cells from germline OCA-B deficient mice mount normal primary T cell responses to lymphocytic choriomeningitis virus (LCMV) but show attenuated CD4<sup>+</sup> memory T cell formation and recall response (21). Elevated *Ocab* (*Pou2af1*) mRNA levels are seen in CD4<sup>+</sup>CD25<sup>lo</sup> early effector cells that are enriched for memory potential (22). OCA-B is also associated with autoimmunity (23–26).

Here, we show that OCA-B deletion in T cells selectively reduces CD4<sup>+</sup> T cell memory potential. We show that ectopic OCA-B expression minimally affects peak CD4<sup>+</sup> T cell responses to LCMV but is sufficient to expand antigen recall responses at the expense of empty vector (EV)-transduced controls. mRNA expression profiling of effector cells ectopically expressing OCA-B reveals gene expression changes associated with effector and memory properties, signaling, and homing. These include global increases in *Socs2* and *Gadd45b*, expansion of short-lived terminal effector T cell populations, and increases in *Tcf7* and *Il7r* in specific memory precursor populations. Using an OCA-B reporter mouse, we show that elevated levels of endogenous OCA-B in effector T cells during the primary response prospectively identify CD4<sup>+</sup> T effector cells with enhanced survival and expansion capability.

## Results and Discussion

**OCA-B in T Cells Is Required for Robust CD4<sup>+</sup> T Cell Memory Recall Response.** We used a conditional *Ocab* (*Pou2af1*) mouse allele crossed to a CD4-Cre driver, which efficiently deletes OCA-B in T cells (26), to study the effects of T cell-specific OCA-B loss. We infected *Ocab*<sup>fl/fl</sup>;CD4-Cre and control *Ocab*<sup>fl/fl</sup> mice with LCMV<sup>Arm</sup> and measured

## Significance

The molecular mechanisms leading to functional CD4<sup>+</sup> T cell memory are incompletely defined and memory progenitors difficult to identify. Here, we show that expression of the Oct coactivator from B cells (OCA-B) transcription coactivator in CD4<sup>+</sup> T cells is necessary and sufficient to drive productive memory. Using a mCherry reporter mouse line, we show that OCA-B expression enriches for responding effector cells with elevated memory potential. The results show that OCA-B expression in T cells is sufficient to promote CD4<sup>+</sup> memory formation and marks memory precursor cells.

Author affiliations: <sup>a</sup>Department of Pathology, University of Utah School of Medicine, Salt Lake City, UT 84112; and <sup>b</sup>Huntsman Cancer Institute, University of Utah School of Medicine, Salt Lake City, UT 84112

Author contributions: J.S.H., M.A.W., and D.T. designed research; W.S., E.P.H., H.K., K.R.C., B.P., J.D., and A.I. performed research; J.S.H. and M.A.W. contributed new reagents/analytic tools; W.S., E.P.H., H.K., J.P., K.R.C., B.P., and A.R.S. analyzed data; and W.S., E.P.H., H.K., J.P., K.R.C., J.D., A.I., J.S.H., M.A.W., and D.T. wrote the paper.

The authors declare no competing interest.

This article is a PNAS Direct Submission.

Copyright © 2024 the Author(s). Published by PNAS. This article is distributed under [Creative Commons Attribution-NonCommercial-NoDerivatives License 4.0 \(CC BY-NC-ND\)](https://creativecommons.org/licenses/by-nc-nd/4.0/).

<sup>1</sup>W.S., E.P.H., and H.K. contributed equally to this work.

<sup>2</sup>Present address: Division of Neuroimmunology Drug Discovery, Janssen Research & Development, Limited Liability Company, San Diego, CA 92121.

<sup>3</sup>Present address: Department of Data Science, Recursion Pharmaceuticals, Salt Lake City, UT 84101.

<sup>4</sup>To whom correspondence may be addressed. Email: dean.tantin@path.utah.edu.

This article contains supporting information online at <https://www.pnas.org/lookup/suppl/doi:10.1073/pnas.2309153121/-DCSupplemental>.

Published February 22, 2024.

specific T cell responses using I-A<sup>b</sup>/gp<sub>66–77</sub> tetramer staining. No significant differences in the frequency of CD4<sup>+</sup> I-A<sup>b</sup>/gp<sub>66–77</sub><sup>+</sup> CD4<sup>+</sup> T cells were observed at 8 d postprimary infection (dpi, *SI Appendix, Fig. S1 A and B*, D8). Rechallenging these mice with *Listeria monocytogenes* expressing the LCMV glycoprotein epitope (Lm-gp61) (27) elicited a trending but nonsignificant decrease in the frequency of cells undergoing memory recall response in *Ocab<sup>fl/fl</sup>;CD4-Cre* mice (*SI Appendix, Fig. S1 A and B*, D40+7). The responding cells did however show a significant decrease in IFN $\gamma$  production (*SI Appendix, Fig. S1 C and D*). The same cells showed minimal changes in ICOS, PD-1, Ly6C or CD62L (*SI Appendix, Fig. S1E*). These results indicate that infection of T cell–conditional OCA-B knockout mice with LCMV results in deficiencies in IFN $\gamma$  expression during memory recall responses.

The relatively small reductions in frequencies of tetramer<sup>+</sup> CD4<sup>+</sup> T cells at recall response may reflect selection for a small percentage of cells escaping OCA-B deletion. This selection can be circumvented using bone marrow chimeras in which conditional deficient or control cells are competed against wild-type T cells in the same mice. We generated bone marrow chimeras in which wild-type donors were coengrafted with congenically marked *Ocab<sup>fl/fl</sup>;CD4-Cre* or control *Ocab<sup>fl/fl</sup>* cells in the same recipients. After 8 wk of engraftment, recipient mice were infected with LCMV. The ratio of antigen-reactive *Ocab<sup>fl/fl</sup>* control effector CD4<sup>+</sup> T cells to wild-type competitor was close to 1:1 at 8 dpi. OCA-B deficient (*Ocab<sup>fl/fl</sup>;CD4-Cre*) cells were slightly reduced relative to wild-type competitor (*SI Appendix, Fig. S1F*). To investigate the effects of T cell–specific OCA-B loss on memory recall responses, we rechallenged mice with Lm-gp61. Following rechallenge, the control to wild-type cell ratio remained close to 1:1 at both primary and memory recall response, while wild-type competitor cells were >eightfold increased at the expense of OCA-B deficient cells specifically at recall (*SI Appendix, Fig. S1 F and G*). These findings indicate that, as with T cell–conditional Oct1 deficiency and global OCA-B deficiency (21), T cell–conditional OCA-B deficiency results in severe deficiencies in CD4<sup>+</sup> T cell memory recall responses.

**Ectopic OCA-B Expression Is Sufficient to Enhance CD4<sup>+</sup> T Cell Memory Responses.** To study the effect of forced OCA-B expression, we primed Ly5.1<sup>+</sup>/5.2<sup>+</sup> (CD45.1<sup>+</sup>45.2<sup>+</sup>) SMARTA TCR transgenic donor mice with GP<sub>61–80</sub> peptide and transduced isolated splenic CD4<sup>+</sup> T cells ex vivo with a retroviral vector expressing mouse OCA-B and GFP. In parallel, Ly5.1<sup>+</sup>/5.1<sup>+</sup> control SMARTA cells were transduced with GFP-expressing EV. SMARTA mice express a transgenic TCR recognizing an immunodominant LCMV glycoprotein (GP<sub>61–80</sub>) CD4<sup>+</sup> epitope (28). GFP<sup>+</sup> SMARTA cells expressing OCA-B and EV controls were sorted, mixed 1:1 and adoptively cotransferred into Ly5.2<sup>+</sup>/5.2<sup>+</sup> recipients (Fig. 1A). Efficient OCA-B expression was confirmed in primary CD4<sup>+</sup> T cells (Fig. 1B). After transfer, recipient mice were infected with LCMV and the cell populations were detected by flow cytometry using congenic markers from the donor T cells and GFP expressed from the viral vector. At 8 dpi, splenic effector EV and OCA-B transduced cells expanded equivalently (Fig. 1 C and D). Another group of mice were infected with LCMV and allowed to clear the virus and form memory. Recall responses were induced by rechallenge using Lm-gp61. At static memory time points (40 dpi) slight but statistically nonsignificant skewing toward the OCA-B population was noted, however at peak T cell response to rechallenge (40+7 dpi), ~50-fold more OCA-B overexpressing SMARTA cells were present (Fig. 1 C–E and *SI Appendix, Fig. S2A*). Although memory recall potential was improved, increases in Tbet and Granzyme B (*Gzmb*), and decreases in CXCR5, Bcl6, and TCF1 at 8 dpi were consistent with an increased Th1 phenotype in OCA-B transduced

cells (Fig. 1 F and G and *SI Appendix, Fig. S2B*). No significant differences in IFN $\gamma$  and Ki-67 were observed at 8 dpi (Fig. 1 H and I). Additionally, IL-7R MFI was significantly decreased in OCA-B expressing cells although cells with strong expression could still be identified (*SI Appendix, Fig. S2C*). The ability of ectopic OCA-B to promote memory recall responses was also observed at longer time points in both the spleen as well as peripheral blood (Fig. 1 J and K and *SI Appendix, Fig. S2D*). These results indicate that OCA-B expression enhances the ability of CD4<sup>+</sup> T cells to induce memory responses.

To investigate whether ectopic OCA-B expression induces gene expression changes in effector cells associated with improved memory recall, we profiled gene expression using splenic SMARTA T cells at 8 dpi. CD4<sup>+</sup> cells were first isolated by magnetic isolation; then, congenically marked GFP<sup>+</sup> cells were further isolated by fluorescence-activated cell sorting (FACS). We identified ~600 down-regulated genes and ~200 up-regulated genes (*Dataset S1*). Unsupervised hierarchical clustering identified differentially expressed gene clusters (Fig. 2A). Down-regulated genes included *Il7r* and *Bcl6*, consistent with the flow cytometry findings at this time point. The top up-regulated gene, *Pou2af1*, encodes OCA-B. Other up-regulated genes were associated with effector activity (*Tbx21* and *Zeb2*), exhaustion (*Irf2l1/Helios*), and attenuation of T cell signaling and proliferation (*Socs2* and *Gadd45b*). *Gadd45b* promotes autoimmune disease and antitumor immune responses (29–32). Example genome tracks are shown in Fig. 2B. Gene ontology (GO) analysis of the up-regulated genes identified terms associated with H3K9me3 regulation. Down-regulated genes by contrast were strongly associated with H3K27me3 in CD4<sup>+</sup> and CD8<sup>+</sup> memory T cells (Fig. 2C). ChIP-X Enrichment Analysis (ChEA) (33) identifies Tp53 and Smc3 as factors that also regulate the gene set induced by OCA-B ectopic expression (Fig. 2D). p53 and SMC3 may therefore also control expression of these genes or could themselves be controlled by OCA-B to regulate gene expression. Sets of significant Molecular Function, Epigenomic Roadmap, and ChEA GO terms are shown in *Dataset S2*.

Effector CD4<sup>+</sup> T cell populations are heterogeneous, with memory progenitor cells comprising a small proportion of the effector T cell population (12, 22, 34). In bulk RNA-seq, increased expression of genes that promote memory in rare memory progenitors may therefore be obscured by decreases in larger populations of terminal effectors. To test this, we performed single-cell RNA-sequencing (scRNA-seq) at D8 post-LCMV infection. Uniform manifold approximation and projection (UMAP) using EV-transduced cells revealed a variety of populations (Fig. 3A and *Dataset S3*). Clusters 1 and 4 were enriched for genes such as *Id3*, *Ccr7*, *Bcl2*, *Slamf6*, and *Tcf7* (both clusters), *Tox* (cluster 1), and *Cxcr5*, *Il7r*, *Icos*, and *Cd69* (cluster 4, *Dataset S3*). These clusters likely contain memory precursor effectors. Clusters 0, 2, and 6 by contrast were enriched in *Ccl5*, *Ifng*, and *Tbx21*, respectively (*Dataset S3*), and likely comprise more terminally differentiated effectors. Cluster 5 showed relative increases in the expression of genes encoding histones, cyclin-dependent kinases and proliferating cell nuclear antigen and likely represent proliferating effectors.

OCA-B-transduced cells clustered more uniformly with fewer clusters (Fig. 3B). Cluster 0 effector cells were marked by *Zeb2*, *Klrg1*, and *Tbx21* (*Dataset S3*). Clusters 1 and 2 were also associated with effector activity. OCA-B transduced cluster 3 was associated with effector/memory progenitor activity similar to EV-transduced clusters 1 and 4 (Fig. 3C). Although there were proportionately fewer of these cells compared to the EV-transduced clusters 1 and 4, multiple memory-associated genes were increased on a per-cell basis. *Tcf7* was increased by >fourfold in OCA-B

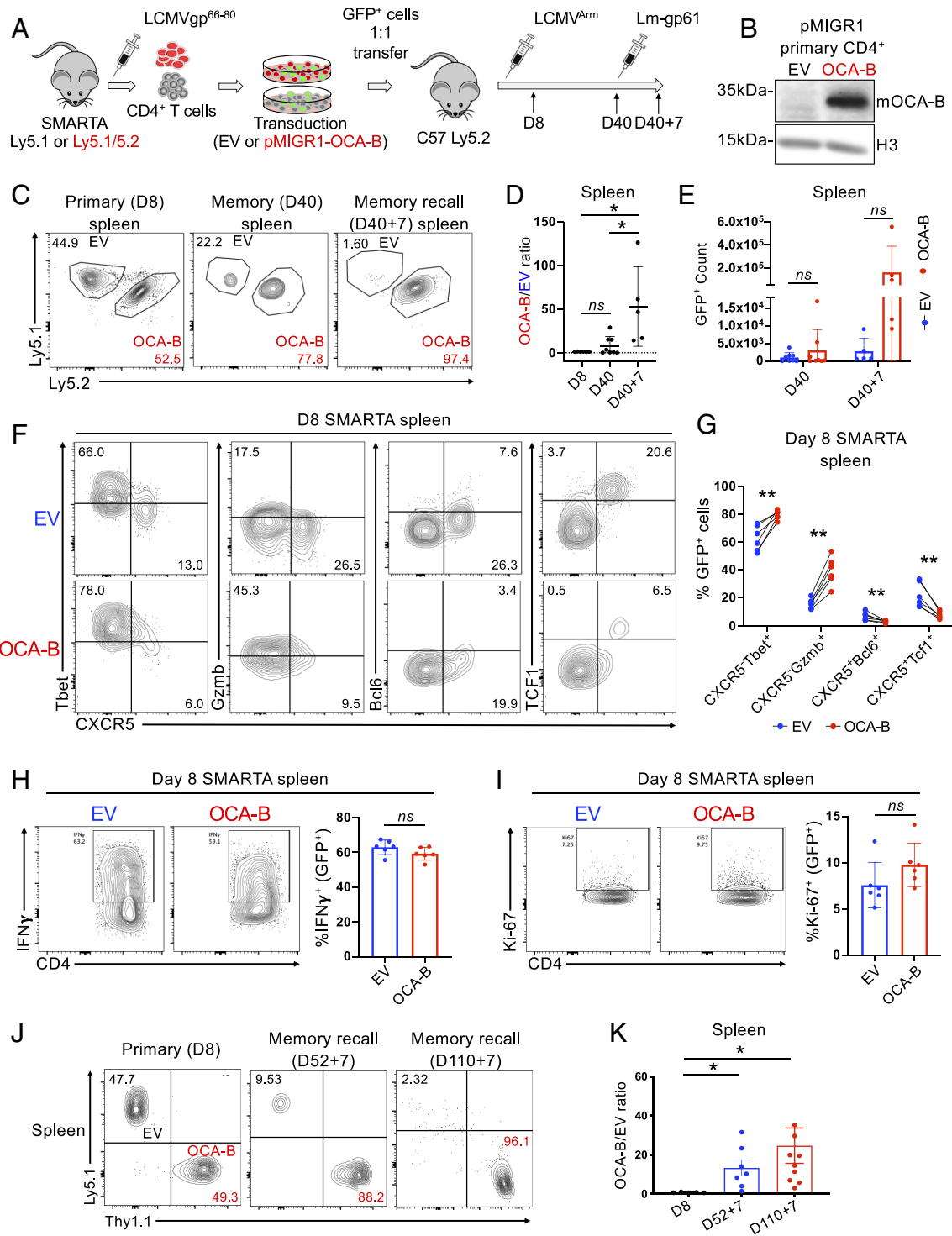


**Fig. 1.** Ectopic OCA-B expression enhances CD4<sup>+</sup> T cell memory recall responses in vivo. (A) Experimental schematic for OCA-B transduction and T cell mixed adoptive transfer. Ly5.1<sup>+</sup> SMARTA cells were transduced with pMSCV-IRES-GFP (pMIGR1, EV), and Ly5.1<sup>+</sup>/5.2<sup>+</sup> SMARTA cells were transduced with pMIGR1 expressing mouse OCA-B (pMIGR1-OCA-B). The donors were age- and sex-matched littermates. Two days following transduction, GFP<sup>+</sup>Ly5.1<sup>+</sup> SMARTA cells (EV) and GFP<sup>+</sup>Ly5.1<sup>+</sup>/5.2<sup>+</sup> SMARTA cells (OCA-B) were sorted, combined 1:1, cotransferred into Ly5.2<sup>+</sup>/5.2<sup>-</sup> C57BL/6J recipient mice, and infected with LCMV. Recipients were tested for static memory on day 40 postinfection and also rechallenge with Lm-gp61 on day 40 analyzed after 7 d. (B) Lysates from primary CD4<sup>+</sup> T cells transduced with either empty pMIGR1 (EV) or pMIGR1-OCA-B were immunoblotted using antibodies against OCA-B. Histone H3 is shown as an internal loading standard. (C) Flow cytometric analysis of Ly5.1<sup>+</sup> pMIGR1 EV-transduced and Ly5.1<sup>+</sup>/5.2<sup>+</sup> pMIGR1-OCA-B-transduced (OCA-B) SMARTA cells in the spleen and blood of a representative recipient mouse at peak effector response (D8), resting memory (D40) and memory recall (D40+7). Live cells were gated based on CD4 and GFP positivity. (D) Ratio of OCA-B/EV transduced cells at D8, D40, and D40+7. (E) GFP<sup>+</sup> cell counts per spleen for EV and OCA-B transduced cells D40 and D40+7 after LCMV infection. (F) D8 response representative flow cytometry plots showing Tbet, Gzmb, Bcl6, Tcf1, and CXCR5 expression in splenic GFP<sup>+</sup> CD4<sup>+</sup> T cells by EV or OCA-B transduction condition. (G) Percentages of CXCR5<sup>+</sup>Tbet<sup>+</sup>, CXCR5<sup>+</sup>Gzmb<sup>+</sup>, CXCR5<sup>+</sup>Bcl6<sup>+</sup>, and CXCR5<sup>+</sup>Tcf1<sup>+</sup> cells comparing EV vs. OCA-B transduction condition at peak response. Individual mice are connected by lines. (H) Representative flow plots and frequency quantification of IFN $\gamma$  producing GFP<sup>+</sup> EV or OCA-B transduced cells. (I) Representative flow plots and frequency quantification of Ki67 producing GFP<sup>+</sup> EV or OCA-B transduced cells. (J) Representative plots showing relative percentages of splenic EV- or pMIGR1-OCA-B-transduced (GFP<sup>+</sup>) SMARTA cells were plotted at D8, D52+7, and 110+7. Each data point represents an individual mouse harboring both EV- and pMIGR1-OCA-B-transduced cells. To obtain measurements from the spleen, 5, 7, and 10 mice were euthanized according to the approved procedure by the University of Utah Institutional Animal Care and Use Committee (IACUC) at each time point. (K) Mean ratios of pMIGR1-OCA-B-transduced relative to EV-transduced SMARTA cells (OCA-B/EV) are plotted. Splenic SMARTA T cells are shown at day 8 postinfection or 7 d post-rechallenge with Lm-gp61 (52+7 or 110+7).

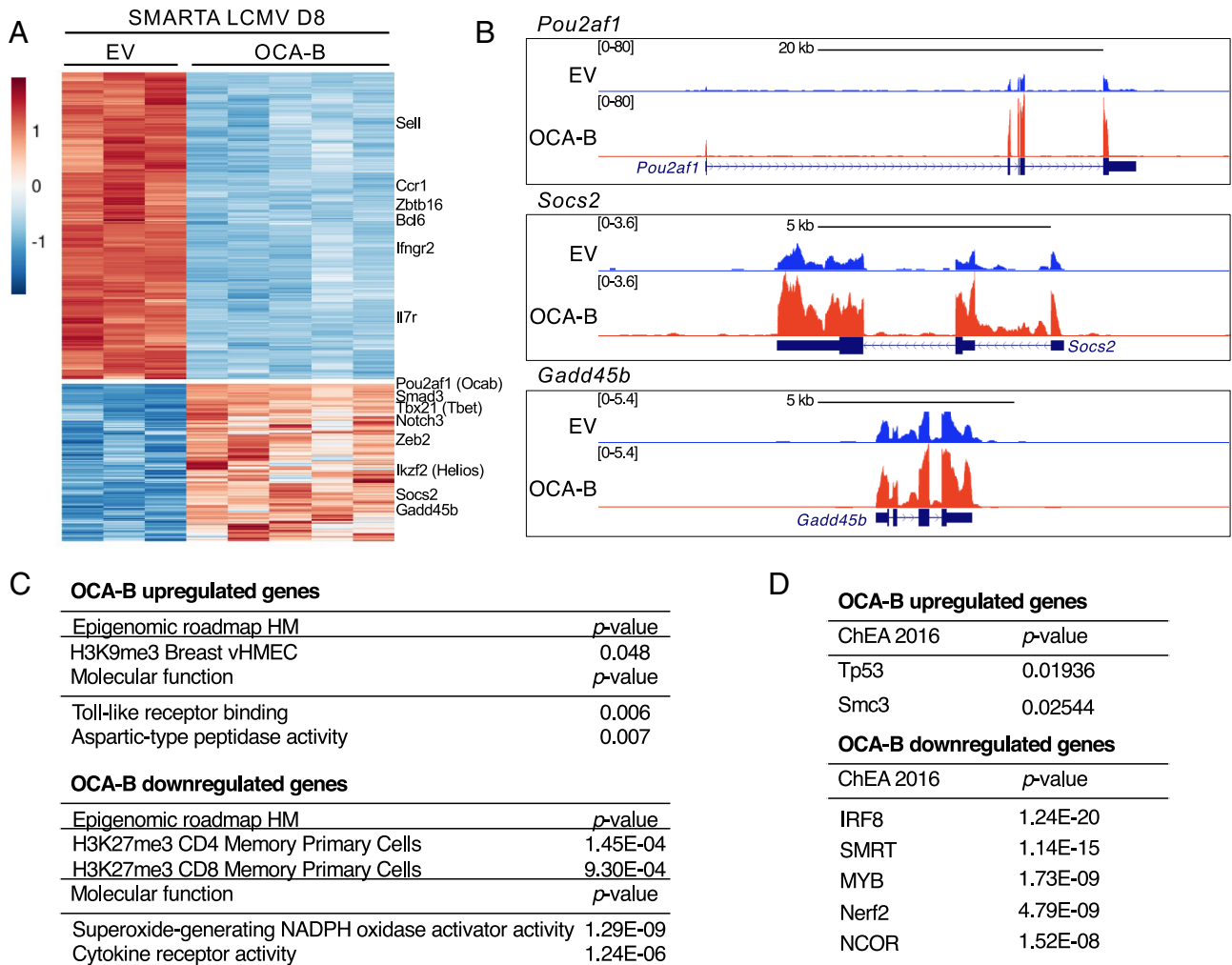


**Fig. 2.** Gene expression changes associated with ectopic OCA-B expression in SMARTA transgenic primary effector T cells. (A) Heatmap showing top up- and down-regulated genes. Genes with  $\log_2$  fold-change  $>0.5$  or  $<-1.0$ , and  $\text{padj} \leq 0.05$  are shown. Example genes are shown at Right. Control and OCA-B-transduced cells were purified from the same mice using magnetic isolation and FACS. (B) Example genome tracks showing two up-regulated genes, *Socs2* and *Gadd45b*. *Pou2af1(Ocab)* is shown as a positive control. (C) Top Epigenomic roadmap and Molecular function GO terms for the set of OCA-B up- and down-regulated genes. (D) Top ChIP-X Enrichment Analysis (ChEA 2016) factors potentially regulating the same set of genes up- and down-regulated by OCA-B ectopic expression.

cluster 3 relative to other clusters, but only twofold in EV clusters 1 and 4 (Dataset S3). *Slamf6* was increased by >threefold in OCA-B cluster 3, but <2.5-fold in EV clusters 1 and 4. *Bcl2* and *Il7r* were similarly more strongly expressed relative to the other clusters in OCA-B- compared to EV-transduced cells. Additionally, *Foxo1* was not overrepresented in either memory-associated EV cluster but was enriched in OCA-B cluster 3, while *Irf2*, which has been associated with CD4<sup>+</sup> T cell exhaustion (35), was not enriched in cluster 3 but was enriched in the equivalent EV-transduced clusters (Dataset S3). *Id3* was enriched in OCA-B-transduced cluster 3 more than EV cluster 4 but less so than in EV cluster 1. These findings suggest that OCA-B transduced cells in cluster 3 are qualitatively superior to their EV-transduced counterparts at forming memory. Simultaneously, OCA-B-transduced clusters showed broad increases in the expression of *Socs2*, which encodes an attenuator of T cell signaling, and *Gadd45b*, which promotes growth arrest (Fig. 3C). These changes likely attenuate effector function and/or may enable a broader transition of effectors to memory progenitors.

Clustering EV- and OCA-B-transduced cells together allows the relative proportions of cells with common gene expression features to be determined. Again, specific clusters were enriched for terminal effectors (Fig. 3D, clusters 0, 1, 2, 4, and 6),

proliferating effectors (cluster 5), and effector cells with memory progenitor potential (cluster 3). Feature plots for genes associated with effector cells (*Tbx21*) and memory function (*Bcl6*) are shown in Fig. 3E. Additional plots for other genes associated with memory are shown in Fig. 3F. In the OCA-B-transduced condition, cluster 3 contained proportionately fewer cells but showed elevated expression of genes such as *Il7r* and *Gadd45b* on a per-cell basis (Fig. 3G). These findings identify changes in gene expression in effector T cell populations consistent with increased memory potential.

**OCA-B Knock-In Reporter Mice Label CD4<sup>+</sup> Memory T Cell Populations.** To monitor OCA-B expression in viable cells, we knocked 3 mCherry reporter cassettes preceded by P2A elements into the mouse *Pou2af1 (Ocab)* locus. The resulting reporter allele contained the mCherry cassettes inserted immediately before the stop codon and the 3'UTR (Fig. 4A). A successful hemizygous knock-in founder and a homozygote generated by intercrossing the progeny were confirmed by PCR (SI Appendix, Fig. S3A). Hemizygous and homozygous reporter mice retained normal OCA-B protein expression (SI Appendix, Fig. S3B). OCA-B was readily detectable in peripheral blood B cells from hemizygous and homozygous reporter mice (SI Appendix, Fig. S3 C and D).

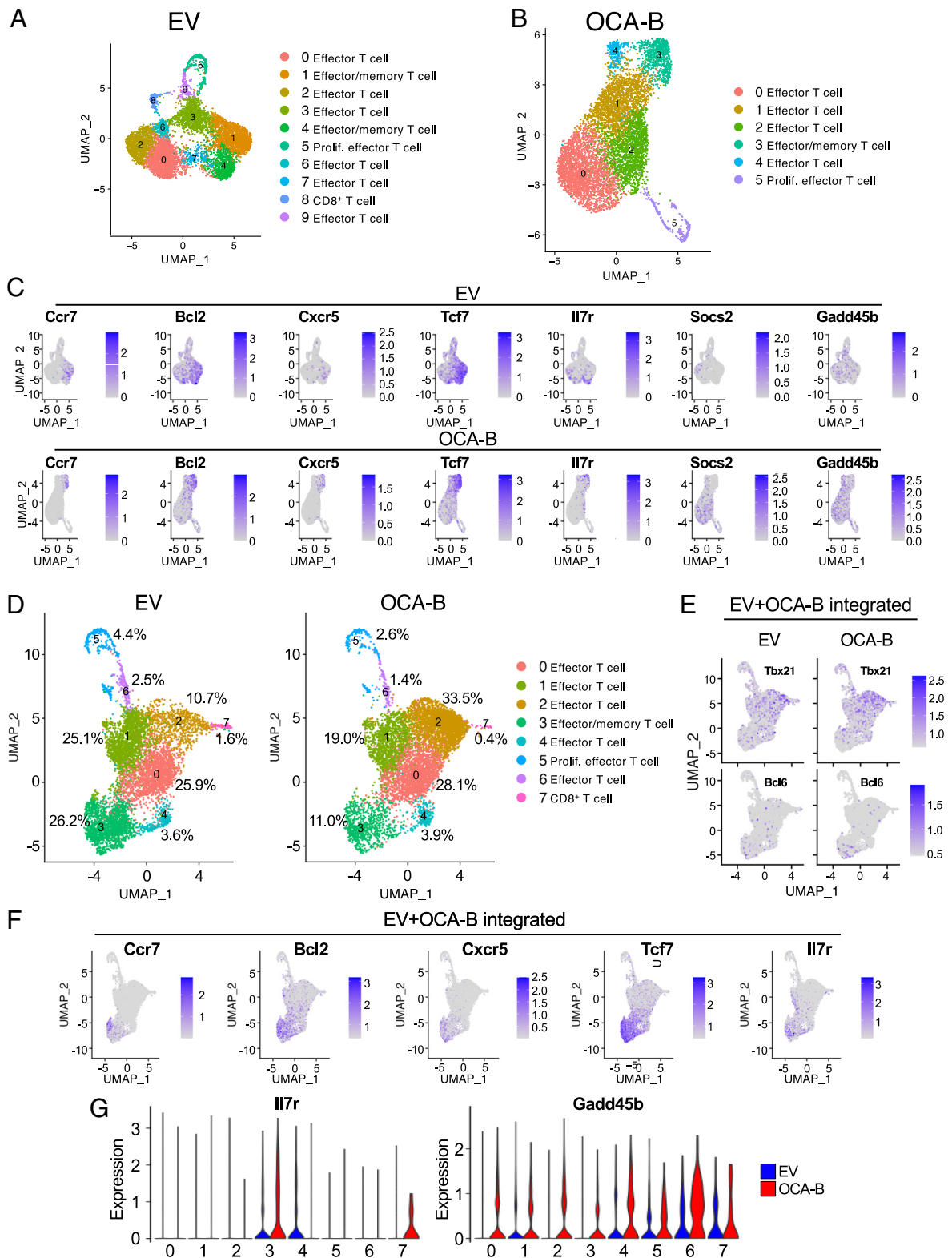


**Fig. 3.** Single-cell RNA-seq analysis of OCA-B-transduced vs. control SMARTA cells at 8 d post-LCMV infection. (A) UMAP projections of independently clustered EV-transduced (GFP<sup>+</sup>) SMARTA cells purified similar to Figs. 2 and 3 and subjected to scRNA-seq. Cluster identities were annotated using a combination of gene expression enrichment (Dataset S3), cluster identity predictor ImmGen identity scores (Dataset S4), and PanglaoDB annotation terms. Clusters 1 and 4 were associated with memory formation. Top PanglaoDB annotation terms for cluster 4 are shown below. (B) Similar UMAP projection using OCA-B-transduced cells purified from the same mice as in (A). Cluster identities were annotated similarly to (A). Cluster 3 in OCA-B-transduced cells was most strongly associated with memory formation. Top PanglaoDB annotation terms for cluster 3 are shown below. (C) Feature plots highlighting expression of representative genes for the two UMAP projections in (A and B). (D) UMAP projections of the EV- and OCA-B-transduced single-cell RNA-seq datasets clustered together. For each projection, the percentage of each cluster relative to the total number of cells is shown. Cluster identities were annotated using a combination of gene expression enrichment (Dataset S3), cluster identity predictor ImmGen identity scores (Dataset S5) and PanglaoDB annotation terms. (E) Feature plots highlighting expression of two representative genes (*Tbx21* and *Bcl6*) associated with specific clusters. (F) Additional combined feature plots supporting the association of cluster 3 with memory progenitors. (G) Violin plots depicting expression of six genes (*Il7r*, *Zeb2*, *Gadd45b*, *Foxo1*, *Tcf7*, and *Tox*) across each of the 10 clusters in EV-transduced cells (blue, Left) and OCA-B-transduced cells (red, Right).

Peripheral T cell expression was weaker, forming a shoulder in hemizygous reporters, but an observable peak in homozygotes (SI Appendix, Fig. S3 C and D). We therefore used heterozygous mice to perform baseline characterization of B cell populations and homozygotes to study T cells.

Robust mCherry expression could be detected in the bone marrow, peritoneal cavity, spleen, and lymph nodes of specific pathogen-free hemizygous reporter mice. Total thymocytes by contrast expressed little OCA-B (SI Appendix, Fig. S3E). OCA-B expression was readily detected in developing, immature, and recirculating B cell populations (SI Appendix, Fig. S3F). Expression was nearly uniform in the different populations, except for a small population of immature B cells that lacked OCA-B expression. Peritoneal B-1 and B-2 B cells were also homogeneous, with stronger expression in B-1 relative to B-2 cells (SI Appendix, Fig. S3G). Splenic B cells can be partitioned into transitional and mature populations. T1/2/3 subsets uniformly expressed OCA-B (SI Appendix, Fig. S3H). Marginal zone (MZ), follicular and non-follicular populations all expressed OCA-B strongly (SI Appendix, Fig. S3I). Expression was largely uniform, but there was a significant population of newly formed CD21<sup>lo</sup>CD23<sup>lo</sup> B cells expressing no OCA-B. The nature and significance of these cells is unknown. These results document strong reporter activity in B cell populations, with the highest level of activity in MZ and B-1 B cells. MZ B cells are largely absent in OCA-B knockout mice (36). These results indicate that the OCA-B reporter robustly labels B cells.

Gating out B cells, approximately 5% of thymocytes from unchallenged, specific pathogen-free homozygous reporter mice expressed OCA-B (SI Appendix, Fig. S3J). mCherry expression could be

identified in CD4/CD8 double-negative (DN), double-positive (DP), and single-positive (SP) compartments, with the highest amounts in DN and CD8 SP cells (SI Appendix, Fig. S3K). In the spleen, the relative abundance of CD4<sup>+</sup> and CD8<sup>+</sup> T cells was unaltered by the reporter allele (Fig. 4B). Splenic CD4<sup>+</sup> T cells express mCherry at ~50-fold lower levels compared to B cells and with a wider range of expression (Fig. 4C). Peripheral blood T cell mCherry levels varied over a similar range (SI Appendix, Fig. S3 C and D).

We used CD62L and CD44 to stratify resting splenic CD4<sup>+</sup> and CD8<sup>+</sup> cells into naive, activated/effector, and central memory compartments. Reporter activity could be detected in approximately 7% of naive (CD62L<sup>hi</sup>CD44<sup>lo</sup>) cells (Fig. 4D). The nature of these cells is unknown. Progressively larger fractions of early activated (CD62L<sup>lo</sup>CD44<sup>lo</sup>), activated (CD62L<sup>lo</sup>CD44<sup>hi</sup>), and T<sub>CM</sub> (CD62L<sup>hi</sup>CD44<sup>hi</sup>) cells expressed mCherry (Fig. 4D). Naive CD8<sup>+</sup> T cells showed comparatively higher expression levels, but decreased expression in the activated state and similar expression in T<sub>CM</sub> cells (Fig. 4E). Therefore, within the CD4<sup>+</sup> T cell compartment, increased OCA-B expression as measured by mCherry fluorescence progressively labels greater fractions of naive, activated, and central memory CD4<sup>+</sup> cells.

**Elevated OCA-B Expression Prospectively Enriches Memory Precursor CD4<sup>+</sup> T Cells.** To assess OCA-B responses during infection, memory formation, and rechallenge, we infected reporter mice with LCMV and used major histocompatibility complex (MHC) tetramers to identify splenic T cells recognizing immunodominant LCMV epitopes. Prior to infection, >90% of cells were CD44<sup>lo</sup> naive phenotype. Up to 30% of cells became CD44<sup>hi</sup> following

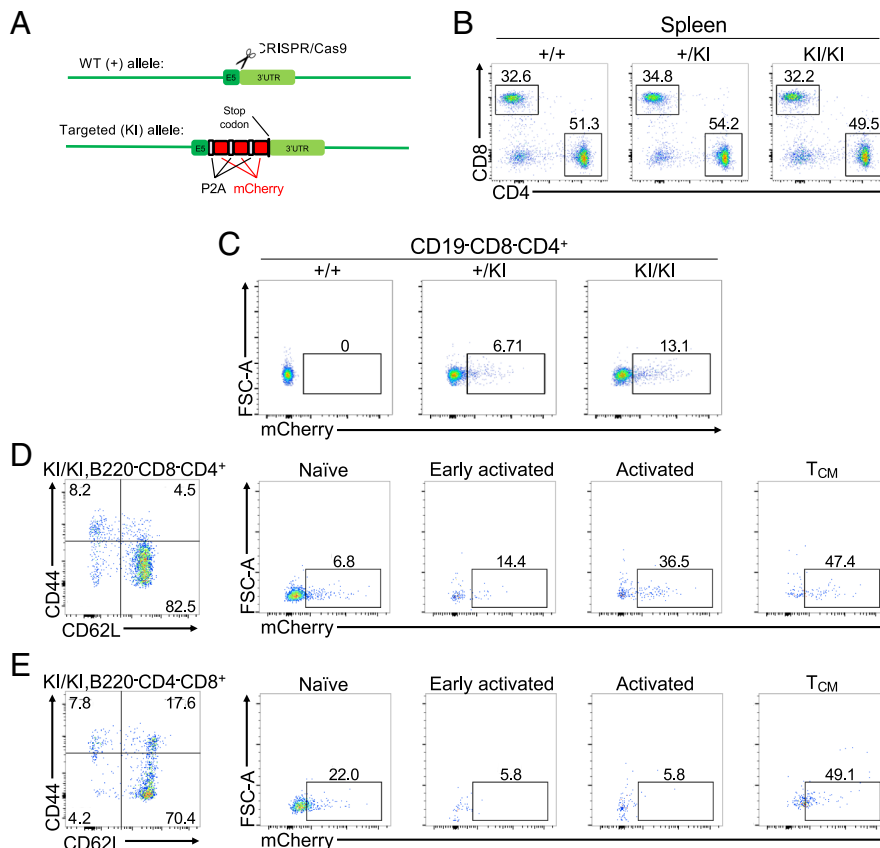


**Fig. 4.** mCherry expression in splenic T cell populations in specific pathogen-free homozygous OCA-B-3×mCherry mice. (A) Mouse *Pou2af1* locus, targeting vector, and the targeted *Pou2af1* locus. (B) CD4 and CD8 expression are shown for an allelic series of example wild-type (+/+) and homozygous (KI/KI) OCA-B knock-in reporter mice. (C) OCA-B homozygous reporter expression in splenic CD4<sup>+</sup> T cell populations. (D) The same CD4<sup>+</sup> cells as in C were further stratified by CD62L and CD44 into naive, early activated, activated, and T<sub>CM</sub> populations. CD62L<sup>lo</sup>CD44<sup>lo</sup> cells are likely recently activated cells that have down-regulated CD62L but not yet up-regulated CD44. (E) Similar analysis as in D except for CD8<sup>+</sup> cells.

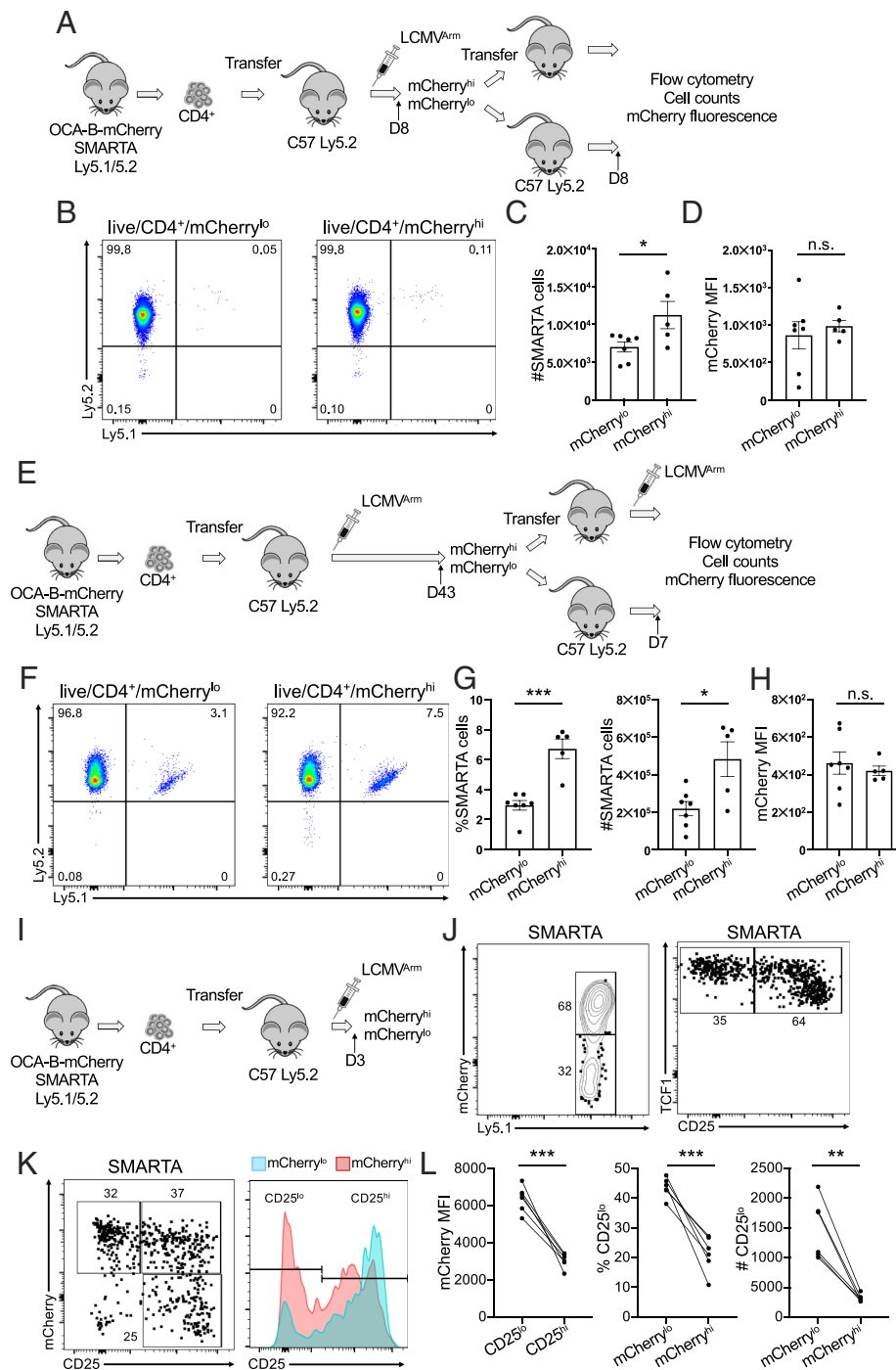


**Fig. 5.** CD4<sup>+</sup> T cells expressing high levels of OCA-B reporter activity preferentially form central memory cells. (A) Schematic for assessing contraction of mCherry<sup>hi</sup> vs. mCherry<sup>lo</sup> SMARTA T cells following LCMV infection. Congenically marked SMARTA T cells were isolated from donor mice, transferred into naive secondary recipients, and infected with LCMV. At 8 dpi, mCherry<sup>hi</sup> and mCherry<sup>lo</sup> populations were isolated by FACS. A total of  $8 \times 10^5$  SMARTA cells were transferred into naive recipients. After 8 d, splenic CD4<sup>+</sup>Ly5.1<sup>+</sup>5.2<sup>+</sup> SMARTA cells were evaluated by flow cytometry. (B) Flow cytometric analysis of SMARTA donor T cells engrafted into naive mice to monitor rates of decline. Representative mice engrafted with mCherry<sup>lo</sup> (Left) or mCherry<sup>hi</sup> (Right) cells are shown. (C) Quantification of averaged donor T cell numbers from mice engrafted with mCherry<sup>lo</sup> or mCherry<sup>hi</sup> cells. N = 7 for the mCherry<sup>lo</sup> group and N = 5 for the mCherry<sup>hi</sup> group. (D) Similar analysis to C except quantifying mean mCherry fluorescence intensity. (E) Schematic for assessing recall responses of mCherry<sup>hi</sup> vs. mCherry<sup>lo</sup> SMARTA T cells following LCMV infection. Congenically marked SMARTA T cells were isolated from donor mice, transferred into naive secondary recipients, and infected with LCMV. However, mice were allowed to clear LCMV and form memory. After 43 d, mCherry<sup>hi</sup> and mCherry<sup>lo</sup> memory T cell populations were isolated by FACS. A total of  $1.3 \times 10^4$  SMARTA cells were transferred into naive recipients, which were infected with LCMV 1 d later. Seven dpi, splenic CD4<sup>+</sup>Ly5.1<sup>+</sup>5.2<sup>+</sup> SMARTA cells were evaluated by flow cytometry. (F) Flow cytometric analysis of SMARTA donor T cells 7 d post-rechallenge to monitor recall responses. Representative mice engrafted with mCherry<sup>lo</sup> (Left) or mCherry<sup>hi</sup> (Right) cells are shown. (G) Quantification of averaged donor T cell percentages and numbers from mice engrafted with mCherry<sup>lo</sup> or mCherry<sup>hi</sup> cells. N = 7 for the mCherry<sup>lo</sup> group and N = 5 for the mCherry<sup>hi</sup> group. (H) Similar analysis to G except quantifying mean mCherry fluorescence intensity. (I) Schematic for assessing mCherry levels in SMARTA T at early time points following LCMV infection. A total of  $2 \times 10^5$  congenically marked (CD45.1<sup>+</sup>) SMARTA T cells were isolated from donor mice and transferred into naive secondary recipients. One day later, mice were intraperitoneally infected with  $2 \times 10^5$  PFU LCMV. Splenic T cells were collected at 3 dpi. (J) Gated unfixed splenic CD4<sup>+</sup> T cells were assessed for the SMARTA congenic marker Ly5.1 and mCherry (Left), while fixed Ly5.1<sup>+</sup> (SMARTA) cells from the same mice were used to assess CD25 and TCF1 (Right). (K) CD25 and mCherry expression were assessed from a representative animal. (Left) distribution of SMARTA cell CD25 and mCherry expression in SMARTA mice. (Right) CD25 levels of gated mCherry<sup>hi</sup> and mCherry<sup>lo</sup> SMARTA cells displayed as a concatenated histogram. (L) Quantification of averaged mCherry MFI in CD25<sup>hi</sup> and CD25<sup>lo</sup> cells (Left) and frequencies (Center) and numbers (Right) of CD25<sup>lo</sup> cells in mCherry<sup>lo</sup> or mCherry<sup>hi</sup> cells SMARTA T cells. N = 6 independent recipient mice.

infection or rechallenge, and a significant number of these were Tet<sup>+</sup> as expected (*SI Appendix, Fig. S4 A, Upper plots*). A high fraction of activated CD44<sup>hi</sup> cells expressed mCherry regardless of tetramer status (*SI Appendix, Fig. S4 A, Lower plots*). mCherry was gated relative to a nonreporter control (*SI Appendix, Fig. S4B*). Fewer activated CD8<sup>+</sup> cells expressed mCherry relative to nonreporter controls (*SI Appendix, Fig. S4 C and D*). After LCMV clearance, memory time point CD4<sup>+</sup> cells maintained high mCherry percentages (*SI Appendix, Fig. S4A, D43, 61.6%*), though with ~twofold lower expression per cell (*SI Appendix, Fig. S4E*). Rechallenge with Lm-gp61 to generate CD4<sup>+</sup> T cell antigen-specific recall responses reduced the percentage of mCherry<sup>+</sup> cells compared to resting memory, with high-affinity tetramer<sup>+</sup> cells declining from >60% to <10% mCherry (*SI Appendix, Fig. S4A, D42+7*). In contrast, a higher percentage of CD8<sup>+</sup> reporter T cells expressed mCherry prior to infection. Higher percentages of tetramer<sup>+</sup>mCherry<sup>+</sup> cells were also present at 5 dpi, but by 8 dpi (peak T cell response) the mCherry percentage was reduced (*SI Appendix, Fig. S4B*). Antigen-specific memory CD8<sup>+</sup> T cells also showed reduced mCherry levels relative to CD4<sup>+</sup> (*SI Appendix, Fig. S4B*). We did not collect data for CD8<sup>+</sup> rechallenge because Lm-gp61 does not express the CD8-dominant epitope recognized by H2-D<sup>b</sup> LCMV tetramers.

To determine whether OCA-B expression in responding CD4<sup>+</sup> T cells is associated with increased memory potential, we crossed the reporter allele to a SMARTA TCR transgenic background to fix the TCR specificity and to Ly5.1 to track engrafted cells. We transferred cells into recipients, infected with LCMV, isolated mCherry<sup>hi</sup> and mCherry<sup>lo</sup> cells at 8 dpi, transferred large numbers of cells ( $8 \times 10^5$ ) into naive secondary recipient mice, and isolated splenic CD4<sup>+</sup> T cells to assess contraction (*Fig. 5A*). mCherry gating for the cells is shown in *SI Appendix, Fig. S4F*. More cells were recovered from mice engrafted with mCherry<sup>hi</sup> cells, indicating that these cells engrafted and/or contracted less than mCherry<sup>lo</sup> controls (*Fig. 5 B and C*). Interestingly the cells that did survive showed similar mCherry levels (*Fig. 5D*). These findings indicate that effector CD4<sup>+</sup> cells expressing higher OCA-B engraft better and/or contract less when transferred into naive animals.

To test the ability of OCA-B expressing cells to mount antigen recall responses, we transferred congenically marked SMARTA cells into recipient mice and infected with LCMV, but instead, mice were allowed to clear virus and form memory. mCherry<sup>hi</sup> and mCherry<sup>lo</sup> cells were collected at 43 dpi. A total of  $4 \times 10^4$  memory SMARTA cells were transferred into naive hosts, which were immediately challenged with LCMV and analyzed at 7 dpi (*Fig. 5E*). mCherry<sup>hi</sup> SMARTA cells responded better compared to mCherry<sup>lo</sup> (*Fig. 5 F and G*) though again with expression normalizing following antigen reencounter (*Fig. 5H*). Example flow cytometry plots are shown in *SI Appendix, Fig. S4G*.

In mice, OCA-B expression can be detected, varying over a 10-fold range, in responding cells as early as 1 d after LCMV infection (21). Memory progenitor cells characterized by low CD25 expression can be identified as early as 3 dpi (15, 22). We transferred SMARTA homozygous OCA-B mCherry reporter T cells into congenic recipients, infected with LCMV, and collected spleens at 3 dpi to study mCherry and CD25 levels (*Fig. 5J*). A large fraction of responding CD25<sup>lo</sup> SMARTA cells expressed mCherry (*Fig. 5J*). SMARTA cells from the same mouse expressing low levels of CD25 also expressed high levels of TCF1, as expected (22). mCherry and TCF1 were not compared as cell fixation quenches mCherry; however, we were able to directly compare CD25 and OCA-B. CD25<sup>hi</sup> cells expressed a range of OCA-B, while CD25<sup>lo</sup> cells were highly enriched for mCherry<sup>hi</sup> cells (*Fig. 5 K and L*). These findings show that high OCA-B expression can be used to prospectively mark live CD4<sup>+</sup> memory precursor effector

T cells with augmented capacity to form central memory. Cumulatively, this study indicates that OCA-B expression within CD4<sup>+</sup> T cells is both necessary for, and sufficient to promote, the emergence of T<sub>CM</sub>.

## Materials and Methods

**Mice.** All mice used in this study were on the C57BL/6J strain background. All mouse experiments were approved by the University of Utah Institutional Animal Care and Use Committee (protocol 00001553). *Pou2af1* (*Ocab*) conditional (floxed) mice were described previously (26). *Pou2af1-3* × mCherry reporter knock-in mice were generated on a C57BL/6N background (Biotocogen) but were backcrossed >5 times to C57BL/6J prior to generation of data herein.

**LCMV and *Listeria* Infection.** LCMV Armstrong 53b (LCMV<sup>Arm</sup>) (37) was grown in BHK cells and titered using Vero cells (28). For primary infection, 8- to 12-wk-old *Ocab*<sup>fl/fl</sup> or *Ocab*<sup>fl/fl</sup>;CD4-Cre mice were inoculated i.p. with  $2 \times 10^5$  plaque-forming units (PFU) of LCMV intraperitoneally.

For heterologous rechallenge with *Listeria monocytogenes* expressing LCMV glycoprotein 61 to 80 (Lm-gp61) (27), bacteria were grown in log phase in BHI media, and concentrations were calculated using OD at 600 nm (OD of 1 =  $1 \times 10^9$  CFU/mL). Mice were rechallenged intravenously (i.v.) with  $2 \times 10^5$  colony forming units (CFU) of Lm-gp61 the indicated number of days after primary infection as published (38).

**Bone Marrow Radiation Chimeras.** Radiation chimeras were generated as published (39). Briefly, male Ly5.1 C57BL/6J mice were used as recipients. Mice received a split dose of 900 Rad ( $2 \times 450$  RAD, spaced 1 h apart) and were engrafted 1 d later with 1 million mixed donor bone marrow cells. Competitor bone marrow cells from Ly5.2/Thy1.1 but otherwise wild-type mice and experimental cells from Ly5.2/Thy1.2 *Ocab*<sup>fl/fl</sup> or littermate *Ocab*<sup>fl/fl</sup>;CD4-Cre mice, were isolated from femurs and tibias of donor mice. After red blood cell lysis, CD3<sup>+</sup> cells were depleted using biotinylated anti-CD3 antibodies (eBioscience) and anti-biotin magnetic MicroBeads (Miltenyi Biotec) according to the manufacturer's instructions. CD3-depleted bone marrow cells were mixed 1:1 and injected retro-orbitally. The chimeras were rested for 8 wk to allow engraftment, after which mice were infected as above. Virus-reactive cells were identified by LCMVgp<sub>66-77</sub>:I-Ab tetramer staining.

**pMSCV-IRES-GFP-OCA-B Vector Generation.** Wild-type *Ocab* cDNA was amplified from the plasmid pcDNA3.1-OCA-B (40) (a gift from Robert Roeder, Rockefeller University, New York, NY) by PCR and cloned into the pMSCV-IRES-GFP (pMIGR1) retroviral vector (a gift from Ryan O'Connell, University of Utah, Salt Lake City, UT). Primers used for amplification were mOcab-F-XhoI, 5'-CTCAGCTGTCTGCTCAAAGAGAAAAGGCAAC; mOcab-R-EcoRI, 5'-GAATTCCTAAAAGCCCTCCACGGAGAGGGT. The PCR product was gel purified, digested with *EcoRI* and *XhoI*, and inserted into a similarly digested pMIGR1 backbone using T4 DNA ligase to generate pMIGR1-OCA-B. All constructs were validated by resequencing.

**CD4<sup>+</sup> T Cell Isolation and Stimulation.** Naive splenic CD4<sup>+</sup> T cells were isolated and stimulated as described previously (41). Briefly, spleens were dissociated by grinding and passing through a 70- $\mu$ m nylon strainer. Red blood cells were lysed by Ammonium-Chloride-Potassium (ACK) lysis buffer (150 mM NH<sub>4</sub>Cl, 10 mM KHCO<sub>3</sub>, and 0.1 mM ethylenediaminetetraacetic acid [EDTA]). Cells were isolated from mice using a naive CD4<sup>+</sup> T cell isolation kit (Miltenyi), and stimulated in culture using 10  $\mu$ g/mL plate-bound anti-CD3 $\epsilon$  and 2  $\mu$ g/mL anti-CD28 antibodies (eBioscience).

**Ectopic OCA-B Expression in CD4<sup>+</sup> T Cells.** Ly5.1<sup>+</sup>/5.1<sup>+</sup> SMARTA and Ly5.1<sup>+</sup>/5.2<sup>+</sup> SMARTA donor mice were i.v. primed with 200  $\mu$ g GP<sub>61-80</sub> peptide (AnaSpec). The next day, T cells were purified using a CD4<sup>+</sup> T cell isolation kit (Miltenyi). Cells were transduced by spin infection with pMIGR retroviruses packaged in 239T cells, with or without mouse OCA-B cDNA. For spin infection, cells were centrifuged with 293T retroviral supernatant at 1,000  $\times$  g for 2 h at 37 °C in the presence of 4  $\mu$ g/mL polybrene (Sigma). Following spin infection, cells were cultured in Roswell Park Memorial Institute (RPMI) 1640 medium supplemented with 10% fetal bovine serum, 50 IU/mL penicillin, 50  $\mu$ g/mL streptomycin, 2 mM L-glutamine, 1 mM sodium pyruvate, 1  $\times$  MEM nonessential amino acids, 55  $\mu$ M 2-mercaptoethanol, and 20 IU/mL recombinant human IL-2 for 2 d. All components were from ThermoFisher with the exception of IL-2, which was supplied by R&D Systems. After 2 d, transduced GFP<sup>+</sup> cells were



isolated by FACS (BD FACSAria). A total of  $1 \times 10^4$  pMIGR1- and pMIGR1-OCA-B-transduced cells were combined and cotransferred into wild-type (Ly5.2/5.2) C57BL/6J mice. Chimeric mice were infected with LCMV and rechallenged with Lm-gp61 as described above. For the experiment shown in Fig. 1 J and K, T cells from Ly5.1 SMARTA and Thy1.1 SMARTA mice were purified using a CD4<sup>+</sup> T cell isolation kit (Miltenyi) and stimulated with CD3 $\epsilon$ /CD28 for 2 d followed by spin transfection.

**Flow Cytometry.** Spleens were dissociated and passed through a 70- $\mu$ m nylon strainer. Red blood cells were lysed by ACK lysis buffer (150 mM NH<sub>4</sub>Cl, 10 mM KHCO<sub>3</sub>, 0.1 mM EDTA). For intracellular staining, cell suspensions in RPMI supplemented with 10% fetal bovine serum were restimulated for 4 h with 1  $\mu$ M LCMV GP<sub>61-80</sub> or 0.1  $\mu$ M GP<sub>33-41</sub> peptide along with Brefeldin A (GolgiPlug Becton-Dickinson, 1  $\mu$ L/mL) as published (42, 43). Cells were subsequently fixed by cell fixation/permeabilization solution (Cytofix/Cytoperm, Becton-Dickinson) according to the manufacturer's protocol. For CXCR5 staining, unstimulated cells were surface stained for 30 min on ice. Cells were subsequently fixed using the FOXP3/Transcription Factor Staining Buffer kit (eBioscience) according to the manufacturer's protocol. Intracellular staining was done in permeabilization buffer for 30 min at room temperature. For tetramer staining, allophycocyanin (APC)-conjugated gp<sub>66-77</sub>-I-A<sup>b</sup> and gp<sub>33-41</sub>:H-2D<sup>b</sup> tetramers were provided by the NIH Tetramer Core Facility (Emory Vaccine Center). Cell suspensions were incubated at 37 °C for 3 h in RPMI with the tetramer followed by cell-surface staining. Tetramer fluorescence was normalized with isotype tetramer (hCLIP:I-A<sup>b</sup>) staining. Fig. 1 C, H, and I were generated using a Cytex Aurora spectral cytometer. All other flow cytometry data were generated using a BD Fortessa LSR. The following anti-mouse antibodies were supplied by eBioscience: CD4-APC (RM4-5), CD3-Biotin (145-2C11), CD90.2-FITC (53-2.1), IL-2-PE (JES6-5H4), IFN $\gamma$ -APC (XMG1.2), CD8a-PerCP/Cy5.5 (53-6.7), and CD90.1/Thy1.1-APC (HIS51). The following antibodies were supplied by BioLegend: CD4-PerCP/Cy5.5 (RM4-5), CD44-APC/Cy7 (IM7), CD278/ICOS-BV510 (C398.4A), CD62L-FITC (MEL-14), CD279/PD-1-BV605 (29F.1A12), CD45.1-PerCP-Cy5.5 (A20), CD45.1-BV711 (104), CD45.2-FITC (104), IgM-APC/Cy7 (RMM-1), B220-APC (RA3-6B2), CD21-PE (7E9), CD23-FITC (B3B4), CD93-APC (AA4.1), CD19-FITC (1D3/CD19), Tbet-APC (4B10), CXCR5-PE-Cy7 (L138D7), CD127/IL7Ra-PE/Cy5 (A7R34), IFN $\gamma$ -APC (XMG1.2), and CD8a-APC (53-6.7). The following antibodies were supplied by BD Biosciences: Ly-6C-BV450 (AL-21), Bcl6-BV421 (k112-91), Tcf1-PE (S33-966), Ki67-V450 (B56), CD4-BUV395 (GK1.5), CD19-BUV661 (ID3), and CD8a-BUV737 (53-6.7). Gzmb-PE (NGZB) was supplied by Invitrogen. Tcf1-AF488 (C63D9) was supplied by Cell Signaling.

**Bulk RNA-seq.** CD4<sup>+</sup> T cells were purified from female Ly5.1 SMARTA and Ly5.1/5.2 SMARTA mice and separately transduced with pMIGR1-OCA-B or pMIGR1 (EV), respectively. On the following day, transduced GFP<sup>+</sup> cells were sorted, 20,000 of each combined 1:1 and injected i.v. into 24 male C57BL/6J male recipients. Twenty-four hours later, each recipient mouse was injected intraperitoneally with  $2 \times 10^5$  pfu LCMV. After 8 d, the 24 mice were divided into six groups of four mice by combining four spleens together. CD4<sup>+</sup> T cells were purified using a Miltenyi CD4 T cell isolation kit. Cells then were stained with PerCP-Cy5.5 Ly5.1 and AF700 Ly5.2 antibodies. GFP<sup>+</sup>Ly5.1<sup>+</sup>Ly5.2<sup>+</sup> (EV) and GFP<sup>+</sup>Ly5.1<sup>+</sup> (OCA-B-expressing) cells were sorted by FACS and used for RNA purification (RNeasy Mini Kit, QIAGEN). RNA concentrations were determined using a Quant-iT RNA assay kit and a Qubit fluorometer (ThermoFisher). Because limited RNA from EV-transduced cells was obtained, the six EV samples were combined into three samples. Five OCA-B-transduced samples (each comprising four mice) were submitted for RNA-seq analysis. These showed a high degree of concordance (not shown). Total RNA samples (200 to 500 ng) were hybridized with Ribo-Zero Plus (Illumina) to deplete cytoplasmic and mitochondrial and ribosomal RNA from samples. RNA-sequencing libraries were prepared as described using the Stranded Total RNA Prep, Ligation with Ribo-Zero Plus kit (Illumina), and IDT for Illumina RNA UD Indexes Set A, Ligation (Illumina). Purified libraries were qualified on an Agilent Technologies 2,200 TapeStation using a D1,000 ScreenTape assay. The molarity of adapter-modified molecules was defined by qPCR using the Kapa Biosystems Kapa Library Quant Kit. Individual libraries were normalized to 0.65 nM in preparation for Illumina sequence analysis. Sequencing libraries were chemically denatured and applied to an Illumina NovaSeq flow cell using the NovaSeq XP workflow (20043131). Following transfer of the flow cell to an Illumina NovaSeq 6,000 instrument, a 150  $\times$  150 cycle paired-end sequence run was performed using a NovaSeq 6000 S4 reagent Kit v1.5 (Illumina).

**Bulk RNA-seq Analysis.** Bulk RNA-seq analysis was performed as previously described (44). Briefly, Reads were aligned to *Mm10* using STAR (v2.7.3a) and checked for quality using multiqc (v1.10). Between 12 and 14 million pair-end reads were generated for each sample, with >98% of aligned reads mapping to the correct strand and >93% of the reads uniquely aligned to the gene. Differentially expressed genes were identified using DESeq2 version 1.24.0 (45) with a 5% FDR cutoff. Features with zero counts and 5 or fewer reads in every sample were removed from the analysis. Genes increased by 1.4-fold or more or decreased by twofold or more and with adjusted  $P < 0.05$  were selected as differentially expressed ( $0.5 < \log_2FC < -1$ ;  $\text{padj} \leq 0.05$ ). Figures were generated in R version 4.0.0 using functions from ggplots libraries and pheatmap.

**ScRNA-seq.** To profile gene expression at the single-cell level, splenic GFP<sup>+</sup>Ly5.1<sup>+</sup>Ly5.2<sup>+</sup> (EV-transduced) and GFP<sup>+</sup>Ly5.1<sup>+</sup> (OCA-B-transduced) SMARTA cells from four pooled mice per condition were isolated, resuspended in PBS with 0.04% bovine serum albumin (ThermoFisher), and filtered through 40- $\mu$ m strainers. Viability and cell count were assessed using Countess II (ThermoFisher). Equilibrium to targeted cell recovery of 6,000 cells along with Gel Beads and reverse transcription reagents were loaded to Chromium Single Cell A to form Gel-bead-in Emulsions (GEMs). Within individual GEMs, cDNA generated from captured and bar-coded mRNA was synthesized by reverse transcription at 53 °C for 45 min. Samples were then heated to 85 °C for 5 min. Single-cell transcriptomes were assessed using a 10 $\times$  Genomics Chromium Single Cell Gene Expression instrument. Individual cells were tagged with 16 bp barcodes and specific transcripts with 10 bp Unique Molecular Identifiers (UMIs) according to manufacturer instructions.

**ScRNA-seq Analysis.** Single-cell transcriptome data were analyzed and clustered as described previously (44). Sequences from the Chromium platform were demultiplexed and aligned using Cell Ranger ver. 3.1.0 (10 $\times$  Genomics) with default parameters mm10-3.0.0. Clustering, filtering, variable gene selection, and dimensionality reduction were performed using Seurat ver. 4.0.4 (46) according to the following workflow: 1, Cells with <200 detected genes were excluded from further analysis. 2, Cells with <5% UMIs mapping to mitochondrial genes and *Cd44* expression >0 were retained for downstream analysis, as SMARTA cells are uniformly responding to LCMV glycoprotein antigen at this time. 3, The UMI counts per ten thousand were log-normalized for each cell using the natural logarithm. 4, Variable genes (2,000 features) were selected using the FindVariableFeatures function. 5, Common anchors between the conditions were identified using FindIntegrationAnchors function that were further used to integrate these sets. 6, Gene expression levels in the integrated set were scaled along each gene, and linear dimensional reduction was performed. The number of principal components was decided through the assessment of statistical plots (JackStrawPlot and ElbowPlot). 7, Cells were clustered using a shared nearest neighbor modularity optimization-based clustering algorithm and visualized using two-dimensional UMAP. 8, One cluster in each condition marked predominantly by mitochondrial genes (indicative of dying cells) was excluded from the analysis. This resulted in 12,886 EV-transduced cells with 45,748 mean reads per cell and 2,595 median genes per cell. The total number of reads was 589,513,069, with 59.6% mapping to exonic regions. Similarly, there were 11,709 OCA-B-transduced cells with 68,931 mean reads per cell, and 2,668 median genes per cell. The total number of reads was 807,111,486, with 57.4% mapping to exonic regions. Clusters were identified using manual interrogation of gene expression enrichment for each population (Dataset S3), the ImmGene cluster identity predictor (Datasets S4 and S5), and PanglaoDB annotation terms. Clusters composed of contaminating macrophages and neutrophils were manually deleted from the visualization.

**Memory Progenitor Isolation, Normalization, and Transfer.** To assess contraction of the effector cells with different OCA-B levels, splenic CD4<sup>+</sup> T cells were purified from 8-wk-old female Ly5.1/5.2 homozygous knock-in reporter, SMARTATCR transgenic mice. A total of  $2 \times 10^4$  SMARTA cells were i.v. injected into 15 male Ly5.2/5.2 C57BL/6J recipients, which were infected intraperitoneally 1 d later with  $2 \times 10^5$  PFU of LCMV in 250  $\mu$ L phosphate-buffered saline. After 8 d, responding Ly5.1<sup>+</sup>5.2<sup>+</sup> SMARTA T cells were sorted into mCherry<sup>hi</sup> and mCherry<sup>lo</sup> populations. Cells were pooled and  $8 \times 10^5$  mCherry<sup>hi</sup> and mCherry<sup>lo</sup> cells were separately injected i.v. into seven naive age-matched 9-wk-old male C57BL/6J secondary recipients in the case of mCherry<sup>lo</sup> and 5 secondary recipients in the case of mCherry<sup>hi</sup>. After

eight additional days, mice were euthanized according to the approved procedure by the University of Utah Institutional Animal Care and Use Committee (IACUC), and splenic Ly5.1<sup>+</sup>5.2<sup>+</sup> SMARTA cells were counted by flow cytometry. To assess proliferative responses to rechallenge, 15 similar virus-naïve secondary recipients were rested for 43 dpi prior to isolation of mCherry<sup>hi</sup> and mCherry<sup>lo</sup> populations. A total of  $1.3 \times 10^4$  SMARTA cells were transferred into naïve recipients, which were infected with LCMV 1 d later. Seven dpi, splenic CD4<sup>+</sup>Ly5.1<sup>+</sup>5.2<sup>+</sup> SMARTA cells were evaluated by flow cytometry. Mice with poor infection/response (total splenocyte count  $<6 \times 10^7$ ) were excluded from the analysis.

**Quantification and Statistical Analysis.** Excel (Microsoft) and Prism (GraphPad) were used for statistics and graphing. Two-tailed Student *t* tests were used to ascribe statistical significance unless otherwise indicated. For all figures, \**P*-value  $\leq 0.05$ ; \*\**P*  $\leq 0.005$ ; \*\*\**P*  $< 0.001$ . All error bars denote  $\pm$  SEM.

1. F. Sallusto, A. Lanzavecchia, K. Araki, R. Ahmed, From vaccines to memory and back. *Immunity* **33**, 451–463 (2010).
2. S. V. Gearty *et al.*, An autoimmune stem-like CD8 T cell population drives type 1 diabetes. *Nature* **602**, 156–161 (2022).
3. A. Schnell *et al.*, Stem-like intestinal Th17 cells give rise to pathogenic effector T cells during autoimmunity. *Cell* **184**, 6281–6298.e23 (2021).
4. P. C. Rosato *et al.*, Virus-specific memory T cells populate tumors and can be repurposed for tumor immunotherapy. *Nat. Commun.* **10**, 567 (2019).
5. G. Cafri *et al.*, Memory T cells targeting oncogenic mutations detected in peripheral blood of epithelial cancer patients. *Nat. Commun.* **10**, 449 (2019).
6. L. A. Shaw *et al.*, Id3 expression identifies CD4(+) memory Th1 cells. *Proc. Natl. Acad. Sci. U.S.A.* **119**, e2204254119 (2022).
7. R. L. Rutishauser *et al.*, Transcriptional repressor Blimp-1 promotes CD8(+) T cell terminal differentiation and represses the acquisition of central memory T cell properties. *Immunity* **31**, 296–308 (2009).
8. A. Kallies, A. Xin, G. T. Belz, S. L. Nutt, Blimp-1 transcription factor is required for the differentiation of effector CD8(+) T cells and memory responses. *Immunity* **31**, 283–295 (2009).
9. H. M. Shin *et al.*, Epigenetic modifications induced by Blimp-1 Regulate CD8(+) T cell memory progression during acute virus infection. *Immunity* **39**, 661–675 (2013).
10. L. Pace *et al.*, The epigenetic control of stemness in CD8(+) T cell fate commitment. *Science* **359**, 177–186 (2018).
11. H. D. Marshall *et al.*, Differential expression of Ly6C and T-bet distinguish effector and memory Th1 CD4(+) cell properties during viral infection. *Immunity* **35**, 633–646 (2011).
12. N. S. Joshi *et al.*, Inflammation directs memory precursor and short-lived effector CD8(+) T cell fates via the graded expression of T-bet transcription factor. *Immunity* **27**, 281–295 (2007).
13. R. Hess Michelini, A. L. Doedens, A. W. Goldrath, S. M. Hedrick, Differentiation of CD8 memory T cells depends on Foxo1. *J. Exp. Med.* **210**, 1189–1200 (2013).
14. R. R. Rao, Q. Li, M. R. Gubbels Bupp, P. A. Shrikant, Transcription factor Foxo1 represses T-bet-mediated effector functions and promotes memory CD8(+) T cell differentiation. *Immunity* **36**, 374–387 (2012).
15. M. Pepper, A. J. Pagan, B. Z. Igyarto, J. J. Taylor, M. K. Jenkins, Opposing signals from the Bcl6 transcription factor and the interleukin-2 receptor generate T helper 1 central and effector memory cells. *Immunity* **35**, 583–595 (2011).
16. H. Ichii *et al.*, Bcl6 is essential for the generation of long-term memory CD4+ T cells. *Int. Immunol.* **19**, 427–433 (2007).
17. A. Banerjee *et al.*, Cutting edge: The transcription factor eomesodermin enables CD8+ T cells to compete for the memory cell niche. *J. Immunol.* **185**, 4988–4992 (2010).
18. D. T. Utschneider *et al.*, T cell factor 1-expressing memory-like CD8(+) T cells sustain the immune response to chronic viral infections. *Immunity* **45**, 415–427 (2016).
19. P. Sauter, P. Matthias, The B cell-specific coactivator OBF-1 (OCA-B, Bob-1) is inducible in T cells and its expression is dispensable for IL-2 gene induction. *Immunobiology* **198**, 207–216 (1997).
20. S. Zwilling, A. Dieckmann, P. Pfisterer, P. Angel, T. Wirth, Inducible expression and phosphorylation of coactivator BOB.1/OBF.1 in T cells. *Science* **277**, 221–225 (1997).
21. A. Shakya *et al.*, Oct1 and OCA-B are selectively required for CD4 memory T cell function. *J. Exp. Med.* **212**, 2115–2131 (2015).
22. J. P. Snook, C. Kim, M. A. Williams, TCR signal strength controls the differentiation of CD4(+) effector and memory T cells. *Sci. Immunol.* **3**, eaas9103 (2018).
23. S. Chevrier, T. Kratina, D. Emslie, A. Karnowski, L. M. Corcoran, Germinal center-independent, IgM-mediated autoimmunity in sanroque mice lacking Obf1. *Immunol. Cell Biol.* **92**, 12–19 (2014).
24. M. Nakamura *et al.*, Genome-wide association study identifies TNFSF15 and POU2AF1 as susceptibility loci for primary biliary cirrhosis in the Japanese population. *Am. J. Hum. Genet.* **91**, 721–728 (2012).
25. M. Ban *et al.*, Linkage disequilibrium screening for multiple sclerosis implicates JAG1 and POU2AF1 as susceptibility genes in Europeans. *J. Neuroimmunol.* **179**, 108–116 (2006).
26. H. Kim *et al.*, Targeting OCA-B/Pou2af1 blocks activated, autoreactive T cells in the pancreas and type-1 diabetes. *J. Exp. Med.* **218**, e20200533 (2021).
27. H. Shen *et al.*, Recombinant *Listeria monocytogenes* as a live vaccine vehicle for the induction of protective anti-viral cell-mediated immunity. *Proc. Natl. Acad. Sci. U.S.A.* **92**, 3987–3991 (1995).
28. A. Oxenius, M. F. Bachmann, R. M. Zinkernagel, H. Hengartner, Virus-specific MHC-class II-restricted TCR-transgenic mice: Effects on humoral and cellular immune responses after viral infection. *Eur. J. Immunol.* **28**, 390–400 (1998).
29. L. Liu *et al.*, Gadd45 beta and Gadd45 gamma are critical for regulating autoimmunity. *J. Exp. Med.* **202**, 1341–1347 (2005).
30. P. Rodriguez-Jimenez *et al.*, Growth arrest and DNA damage-inducible proteins (GADD45) in psoriasis. *Sci. Rep.* **11**, 14579 (2021).
31. Y. Luo *et al.*, Suppression of collagen-induced arthritis in growth arrest and DNA damage-inducible protein 45beta-deficient mice. *Arthritis Rheum.* **63**, 2949–2955 (2011).
32. S. Ju *et al.*, Gadd45b and Gadd45g are important for anti-tumor immune responses. *Eur. J. Immunol.* **39**, 3010–3018 (2009).
33. A. Lachmann *et al.*, ChEA: Transcription factor regulation inferred from integrating genome-wide ChIP-X experiments. *Bioinformatics* **26**, 2438–2444 (2010).
34. J. N. Blattman *et al.*, Estimating the precursor frequency of naive antigen-specific CD8 T cells. *J. Exp. Med.* **195**, 657–664 (2002).
35. A. Crawford *et al.*, Molecular and transcriptional basis of CD4(+) T cell dysfunction during chronic infection. *Immunity* **40**, 289–302 (2014).
36. T. Samardzic, D. Marinkovic, P. J. Nielsen, L. Nitschke, T. Wirth, BOB.1/OBF.1 deficiency affects marginal-zone B-cell compartment. *Mol. Cell Biol.* **22**, 8320–8331 (2002).
37. R. Ahmed, A. Salmi, L. D. Butler, J. M. Chiller, M. B. Oldstone, Selection of genetic variants of lymphocytic choriomeningitis virus in spleens of persistently infected mice. Role in suppression of cytotoxic T lymphocyte response and viral persistence. *J. Exp. Med.* **160**, 521–540 (1984).
38. C. Kim, D. C. Jay, M. A. Williams, Stability and function of secondary Th1 memory cells are dependent on the nature of the secondary stimulus. *J. Immunol.* **189**, 2348–2355 (2012).
39. D. M. Mitchell, E. V. Ravkov, M. A. Williams, Distinct roles for IL-2 and IL-15 in the differentiation and survival of CD8+ effector and memory T cells. *J. Immunol.* **184**, 6719–6730 (2010).
40. Y. Luo, R. G. Roeder, Cloning, functional characterization, and mechanism of action of the B-cell-specific transcriptional coactivator OCA-B. *Mol. Cell Biol.* **15**, 4115–4124 (1995).
41. A. Shakya, J. Kang, J. Chumley, M. A. Williams, D. Tantin, Oct1 is a switchable, bipotential stabilizer of repressed and inducible transcriptional states. *J. Biol. Chem.* **286**, 450–459 (2011).
42. K. Murali-Krishna *et al.*, Counting antigen-specific CD8 T cells: A reevaluation of bystander activation during viral infection. *Immunity* **8**, 177–187 (1998).
43. M. A. Williams, E. V. Ravkov, M. J. Bevan, Rapid culling of the CD4+ T cell repertoire in the transition from effector to memory. *Immunity* **28**, 533–545 (2008).
44. J. Perovanovic *et al.*, Oct1 cooperates with the Smad family of transcription factors to promote mesodermal lineage specification. *Sci. Signal.* **16**, eadd5750 (2023).
45. M. I. Love, W. Huber, S. Anders, Moderated estimation of fold change and dispersion for RNA seq data with DESeq2. *Genome Biol.* **15**, 550 (2014).
46. T. Stuart *et al.*, Comprehensive integration of single-cell data. *Cell* **177**, 1888–1902.e21 (2019).
47. D. Tantin, Data from "OCA-B/Pou2af1 is sufficient to promote CD4 memory and prospectively identifies memory precursors." NCBI Gene Expression Omnibus (GEO). Available at <https://www.ncbi.nlm.nih.gov/geo/query/acc.cgi?acc=GSE214310>. Deposited 27 September 2022.

**Data, Materials, and Software Availability.** Materials used in the study are available to any researcher for purposes of reproducing or extending the findings (47). Bulk and single-cell RNA seq data have been deposited at the Gene Expression Omnibus (GEO) website (<https://www.ncbi.nlm.nih.gov/geo/> and [GSE214310](https://www.ncbi.nlm.nih.gov/geo/)). All other data are available in the main text or [supporting information](#).

**ACKNOWLEDGMENTS.** We thank M. Chandrasekharan for help with graphics. We thank J. Marvin and the University of Utah Health Sciences Center Flow Cytometry Core facility. We thank O. Allen, B. Dalley, and the High-Throughput Genomics Core. MHC tetramers were provided by the NIH Tetramer Core Facility (Atlanta, GA). We thank R. Roeder for the mouse OCA-B cDNA and R. M. O'Connell for the pMIGR1 plasmid. This work was supported by NIH grants R01AI100873 and R01AI162929 to D.T.